Construction and Building Materials 458 (2025) 139556

Contents lists available at ScienceDirect

Construction and Building Materials

journal homepage: www.elsevier.com/locate/conbuildmat

Radon diffusion coefficient of cement pastes made with recycled thermal carbon fly ashes

E. Castaño-Casco [a,*,1], A. Caño [b,1], J.A. Suárez-Navarro [c], I. Gutiérrez-Álvarez [a], A. Barba-Lobo [a], J.P. Bolívar [a], M.M. Alonso [b]

[a] Radiation Physics and Environment Group (FRYMA), Centre for Natural Resources, Health and Environment (RENSMA), University of Huelva, Huelva 21007, Spain
[b] Eduardo Torroja Institute for Construction Sciences (IETcc-CSIC), Madrid 28033, Spain
[c] Environmental Radioactivity and Radiological Monitoring Unit (URAyVR), Energy, Environment and Technology Research Centre (CIEMAT), Madrid 28020, Spain

ARTICLE INFO

Keywords:
Cement
Fly ash
Radon
Radon diffusion coefficient
Characterization
Gamma spectrometry

ABSTRACT

The use of supplementary cementitious materials (SCMs) is one of the most used ways to reduce CO_2 emissions associated with the production of Portland cement. However, many of these SCMs are Naturally Occurring Radioactive Materials (NORM), which present naturally occurring radionuclides. Radon emission from these types of materials, together with radon infiltration from the ground through them, is one of the main sources of indoor radon. These pathways through the building materials are regulated by the radon diffusion coefficient, *D*. In this work, the radon properties of 7 cement pastes (at 2 and 28 days) were studied in function of the technical properties to determine their suitability as building and insulating materials against radon. Two main results were found: The *D* of the pastes changed by an order of magnitude between those with a 2-day curing time and those with a 28-day curing time, the latter being less permeable to radon, and there was also a decrease in *D* as the percentage of superplasticiser admixture increased, due to the reduction in the porosity of the final pastes and the reduction in radon permeability. The lowest *D* value obtained was of $(4.3 \pm 0.4) \cdot 10^{-11}$ m^2 s^{-1} for the paste with a 70% of cement, 30% of fly ash, 0.6% of superplasticiser admixture and 28 days of curing. In conclusion, it was found that different characteristics of the paste production, which influence the final microstructure, can produce cements containing NORM with permeabilities to radon low enough to be used as a radon barrier.

1. Introduction

Although the construction sector is an important economic and social actor on a global scale, it has a large energy and environmental impact. The manufacture of different building materials leads to the emission of large quantities of greenhouse gases (GHG), specifically CO_2, into the atmosphere [1]. Concrete, which is the main building material and the most widely used human-made material in the world, has as its main component Portland Cement (PC), which is mainly composed of a material called clinker. The manufacture of this clinker requires large amounts of both raw materials and energy, and it is estimated that for every tonne (1000 kg) of clinker produced, 0.8 tonnes of CO_2 are emitted into the atmosphere, representing about 7% of global anthropogenic CO_2 emissions worldwide [2].

One of the most important strategies to mitigate this negative effect is the production of cements with low clinker content and its substitution by Secondary Cementitious Materials (SCM) [3–5], which are in many cases waste or industrial by-products, such as blast furnace slag, silica fume, natural pozzolans, fly ash, etc as well as promising new SCMs such as biomass ashes, new pozzolanic materials, sludges of different nature etc. [6,7] that are not yet covered by European standards [8].

However, the use of these SCMs or other types of waste or alternative materials must guarantee that: a) the technical specifications of each building material are met, and b) their use does not pose any risk to the health of living beings or to the environment. In many cases these waste and materials pose a higher content of natural radionuclides than those normally found in nature, which could imply an undesirable radiological risk. These materials can be a) geological materials with a high concentration of natural radionuclide activity, such as granites, basaltic rocks or sedimentary rocks like clays, sandstones or limestones; b) NORM wastes or 'Naturally Occurring Radioactive Materials', which are

* Corresponding author.
E-mail address: elena.castano@dci.uhu.es (E. Castaño-Casco).
[1] These authors share first authorship in this work

https://doi.org/10.1016/j.conbuildmat.2024.139556
Received 6 September 2024; Received in revised form 14 November 2024; Accepted 10 December 2024

wastes from mining or industrial manufacturing that have an increased concentration of naturally occurring radionuclides compared to the raw materials [9,10]. These NORM wastes include many of the current additions to cement, such as fly ash (FA) or blast furnace slag (S), or other wastes that are included in non-conventional sustainable cementitious materials (phosphogypsum, red mud, slags, etc.) or mining sludge wastes used in the manufacture of mortar and concrete.

The natural radionuclides are those belonging to the natural radioactive series ^{238}U, ^{235}U and ^{232}Th, together with ^{40}K, present in almost all constituents of the earth's crust. These radionuclides are responsible for the natural dose received by humans together with cosmic radiation. The effective natural dose to a person is due to external exposure from gamma radiation, ingestion and inhalation from radon daughters in the air.

^{222}Rn is a radioactive short-lived ($T_{1/2}$ = 3.82 d) gas from the naturally occurring radioactive chain from ^{238}U. This gas emanates from the solid grains and then can migrate into the surface of the material and escape into the atmospheric air [11,12]. Radon is diluted in the atmosphere reaching in outdoors surface air concentrations around 10 Bq m^{-3}, but indoors it can accumulate and reach levels up to 3 orders of magnitude higher [13,14]. Radon decays in the air into its four short-lived radionuclides, which are generally attached onto the atmospheric aerosols, and can be inhaled generating a radiological exposition to tissues. Long-term inhalation under high concentrations increases significantly the lung cancer risk, being the second most common cause after tobacco [15–17].

International organizations such as the International Commission on Radiological Protection (ICRP) or the World Health Organisation (WHO) advocate international programmes to reduce the risk of radon to the public [18,19]. The new European Directive 2013/59/EURATOM [20] on basic safety standards include radon requirements to reduce the public exposure to radon, requiring Member States to elaborate national plans against radon and to establish a national reference value for radon concentration in close buildings, with the reference value being an annual average of less than 300 Bq m^{-3}. In Spain, this requirement is included in the Technical Building Code [21], where the basic requirement of protection against radon appears, stating that buildings shall have adequate means to limit the foreseeable risk of excessive exposure to radon in enclosed spaces.

Radon can accumulate inside buildings through three mechanisms [22]: a) soil gas convection through cracks and fissures, b) soil gas diffusion from the ground through the porosity of building materials and c) exhalation from building materials d) outdoor air and tap water. However, the main source of indoor radon [23,24] is the infiltration from the soil of the building basement, through cracks and crevices, or by diffusion through the construction elements [25–27]. The building materials themselves, depending on their radioactive composition [28,29], can also generate radon and release it into the indoor air [30–32]. To achieve the objectives of the Directive, it is necessary to ensure the reliability of measurements of the radon concentration in air, the radon exhalation rate and the radon diffusion coefficient in a way that is simple, robust and easy to replicate. The determination of the radon diffusion coefficient of construction elements is essential to control the radon exhalation rate on indoor surfaces and to ensure that the radon concentration is below the recommended levels. For this reason, it is necessary to find building and insulation materials [33–36], that is materials designed to have a low radon permeability, to reduce indoor radon concentrations [37].

There are several methods for determining the radon diffusion coefficient [38]. Some of them use indirect measurement, by using two activated charcoal canisters, one of which is covered with the problem material, and exposing them to a known radon concentration [39], or by covering one side of a modified Lucas cell, also containing a radon source, with the problem material and studying the decay of the radon concentration [40,41]. Others use direct measurements to study the exhalation rate from one side of the material and obtain the radon diffusion coefficient assuming a steady state [42,43], and there are also non-experimental methods using Monte Carlo simulation [44]. There is also an existing ISO norm for the determination of the radon diffusion coefficient, ISO 11665–13 [45], which is based on the work of [46]. The methodology relies on the measurement of the radon concentration in two chambers separated by the problem material. A radon source is placed in one of the chambers and the other one is kept empty, and this difference in concentration will generate a diffusion transport through the problem material. In [47] an algorithm has been developed in order to make the methodology easier to apply and replicate.

Radon insulation layers are usually placed on mortar and concrete, the lower the radon diffusion through them, the higher the effectiveness of the insulation system. In Spain protective barriers must ensure that the radon diffusion coefficient is less than 10^{-11} m^2 s^{-1} [21], but there is not an international or European standard [48]. Other examples of regulations are in Ireland, where the radon diffusion coefficient must be less than 10^{-12} m^2 s^{-1} [49], or countries with a regulation on the thickness of the radon barrier, like Germany, less than 3 times its diffusion length [50], or the Czech Republic, less than a parameter that depends on the building and soil characteristics [51]. There are also previous studies on radon exhalation from different building materials, some of which incorporated fly ash into concretes [52,53]. However, our study has gone further by assessing the possibility that these materials, while exhaling radon, can serve as insulating materials in cases where there is an elevated radon source in the soil at the building foundation. In this work a new methodology has been applied to measure the radon diffusion coefficient [47] of cement pastes with different percentages of fly ash and a superplasticiser admixture. In this way, this work has addressed both the need to solve the problem of reducing cement production by using SCMs and the need to find materials with a low radon diffusion coefficient to use as radon barriers.

2. Materials and methods

2.1. Materials

The following materials were used in this study: I) a CEM I 42.5 R and (CEM), II) a F-type fly ash (FA) (ASTM C618) from the coal combustion in a thermoelectric power plant located in Teruel (Spain). Additionally, in some of the mixtures specified in the following section, a Sika ViscoCrete superplasticiser admixture based on polycarboxylates (PCE) was added.

The chemical analysis of both the starting materials was carried out by X-ray fluorescence (XRF) (S8 Tiger Bruker) (Table 1).

As it can be seen in Table 1, the predominant oxides in the CEM are CaO (63.78%), SiO_2 (19.84%), Al_2O_3 (5.38%) and Fe_2O_3 (2.43%), while in the FA, the main oxides are SiO_2 (41.55%), Al_2O_3 (22.97%) and Fe_2O_3 (23.26%). These compositions are in agreement with previous studies [54,55].

Mineralogical composition was carried out by X-ray diffraction (XRD) using a BRUKER-AXS D8 ADVANCE diffractometer. The recording conditions were in the range 2θ values of 5–60º with a step/size equal to 0.019736º and a time/step of 0.5 s and using Cu-Kα1 radiation. For the analysis of the diffractograms, the Diffract Plus EVA (Fig. 1). The main phases identified for CEM were gypsum, quartz, alite, belite, C_3A and C_4AF, all of which are common in type I cements. For the FA, the identified phases were quartz, mullite, hematite, magnetite, magnesioferrite, maghemite and lime. In addition, the presence of an amorphous halo is observed between the 15–35° 2θ angles, corresponding to the presence of amorphous content.

Particle size distribution of CEM and FA, were determined by laser diffraction with a S. Malvern Mastersizer with isopropanol as dispersing medium, and BET area values were determined on a Micromeritics ASAP 2000. Table 2 presents the results of the particle size distribution for CEM and FA, graphically represented in Fig. 2. The CEM used shows a particle size distribution, with 90% of the particles below 27 μm, 50%

Table 1
Chemical composition (% wt.) of CEM and FA.

	SiO_2	Al_2O_3	Fe_2O_3	CaO	MgO	TiO_2	Na_2O	K_2O	P_2O_5
CEM	19.84	5.38	2.43	63.78	1.48	0.24	0.04	0.70	0.09
FA	41.55	22.97	23.26	6.37	0.70	0.95	0.35	1.33	0.13
	SO_3	**MnO**	**SrO**	**ZrO_2**	**ZnO**	**BaO**	**Cl**	**Cr_2O_3**	**LoI***
CEM	3.33	0.07	0.06	-	0.05	0.04	0.01	0.01	2.78
FA	0.75	0.06	0.05	0.03	0.02	-	-	0.03	1.42

* LoI. Loss on ignition (1000ºC)

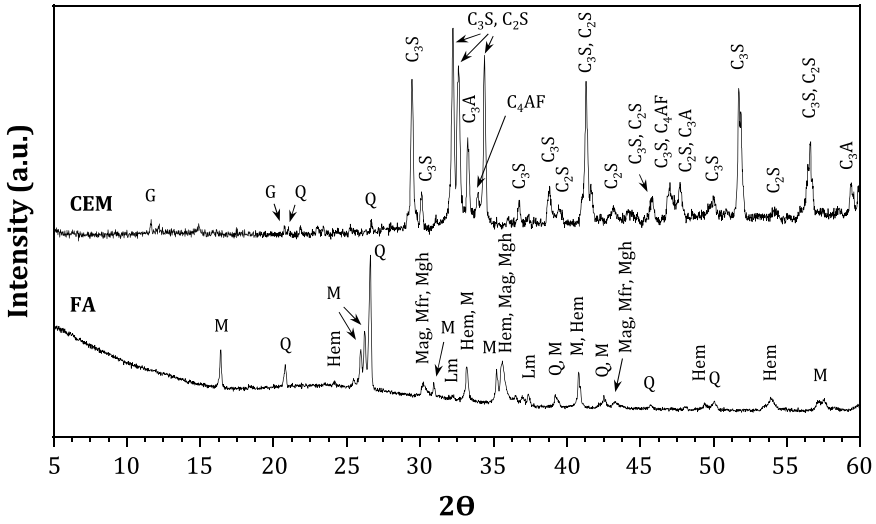

Fig. 1. Diffractograms of the CEM and FA used for the cement pastes preparation. G: Gypsum ($CaSO_4{\cdot}2\ H_2O$) (COD 9015350), Q: Quartz (SIO_2) (COD 9009666), C_3S: Alite ($3CaO{\cdot}SiO_2$) (COD 1540704), C_2S: Belite ($2CaO{\cdot}SiO_2$) (COD 9012789), C_3A: Tricalcium Aluminate ($3CaO{\cdot}Al_2O_3$) (COD 9014359), C_4AF: Brownmillerite (Calcium Aluminoferrite) ($4CaO{\cdot}Fe_2O_3{\cdot}Al_2O_3$) (COD 1008724), M: Mullite ($Al_{4+2x}Si_{2-2x}O_{10-x}$) (COD 7105575), Hem: Hematite ($Fe_2^{3+}O_3$) (COD 9015964), Mag: Magnetite ($Fe^{2+}Fe_2^{3+}O_4$) (COD 9005812), Mfr: Magnesioferrite ($Mg(Fe^{3+})_2O_4$) (COD 9007273), Mgh: Maghemite ($Fe_2^{3+}O_3$) (COD 9006318), Lm: Lime (CaO) (COD 1000044).

Table 2
Particle size distribution of CEM and FA at the 10th, 50th and 90th percentiles, together with their specific surface area obtained by BET.

	Dv (10) μm	Dv (50) μm	Dv (90) μm	Degassing conditions	BET area (m^2/g)
CEM	1.29	8.51	27.0	50ºC/16H	2.33
FA	1.82	7.81	30.6	50ºC/16H	4.10

below 8.51 μm and, for the remaining 10%, a bottom particle size of under 1.29 μm. On the other hand, FA had a bimodal distribution centred on two particle size peaks, 16.40 and 4.58 μm. However, 90% of the FA particles were below 30.06 μm, 50% below 7.81 μm, and a percentage of 10% of particles under 1.82 μm.

The average specific surface area of the particles of CEM and FA, were analysed by the BET method (ASAP 2420 Micromeritics), and it was found that the particles of FA have a higher specific surface area than those of CEM (Table 2).

2.2. Design and sample preparation of pastes specimens

In this study, seven different cement paste blends were prepared by increasing the percentage of replacement of cement (CEM) with fly ash (FA). Two of the prepared blends included the addition of superplasticiser admixtures in different proportions on the weight of solid.

Table 3 shows the proportions (% weight) of the raw materials used in each blend, as well as the liquid/solid ratio used, which was kept constant for all blends, with the exception of those that included superplasticiser admixture, which considerably decreases the water demand. Therefore, in order to compare all the samples, all blends were prepared with the necessary liquid/solid ratio to reach same consistency in all pastes. The consistency of the different blends was determined by performing a normal consistency test according to the standard UNE-EN 196–3:2017 [56].

To prepare the different blends and prior to the addition of water, the CEM and the FA were mixed and homogenised in a blender machine (T2C TURBULA®, WAB) for 1 hour at 34 rpm. For the samples containing superplasticiser admixture (PCE), this was added to the water and homogenised previously. The pastes were placed in different moulds:

- Seven cubic moulds with dimensions of $5 \times 5 \times 5\ cm^3$
- Four cubic moulds of $3 \times 3 \times 3\ cm^3$
- and one mould of $1 \times 10 \times 10\ cm^3$. The latter mould in slab geometry was prepared specifically for this study by means of a 3D printer using polypropylene as the material, so as to adapt to the proposed methodology for the measurement of the radon diffusion coefficient.

The samples were cured in a climatic chamber (25°C and 99% RH) during 20 h. Afterwards the specimens were demoulded and kept under the same conditions for a curing time of 2 and 28 days.

As an example, Fig. 3 shows the specimens prepared for one of the pastes made.

2.3. Characterization of the pastes: mechanical performance, physical characteristics and microstructure of the pastes

The mechanical compressive strength of each blend, at ages of 2 and 28 days, was carried out using an Ibertest Autotest-200/10-SW press.

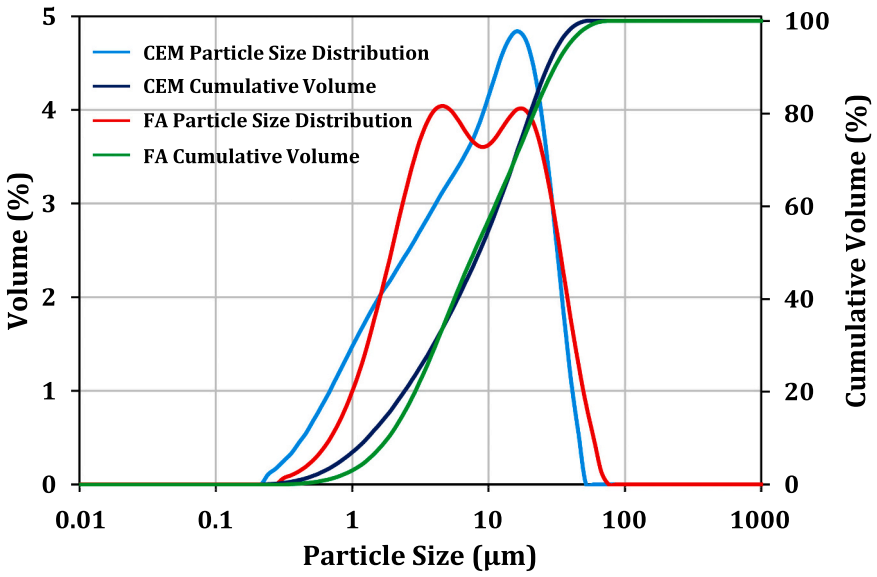

Fig. 2. Particle size distribution and cumulative distribution of the CEM and FA.

Table 3
Code of the sample depending on the composition and curing time. For example, for a composition of 70% of cement, 30% of fly ash, 0.4% of admixture plasticiser and 2 days of curing time the code will be 70–30-04SP-2. When the plasticiser is not added, its position in the code is removed as the case of 100–0-28.

Code	CEM (%)	FA (%)	SP (%)[a]	Curing Time (days)	l/s*
100–0–2	100	0	-	2	0.29
100–0–28				28	
90–10–2	90	10	-	2	0.29
90–10–28				28	
80–20–2	80	20	-	2	0.29
80–20–28				28	
70–30–2	70	30	-	2	0.29
70–30–28				28	
60–40–2	60	40	-	2	0.29
60–40–28				28	
70–30–04SP–2	70	30	0.4	2	0.23
70–30–04SP–28				28	
70–30–06SP–2	70	30	0.6	2	0.22
70–30–06SP–28				28	

[a] % of CEM + FA total weight.
* l/s = liquid solid ratio.

For this purpose, three specimens of 5 × 5×5 cm^3 dimensions per blend and curing time were used, being the final result the mean value and the error the standard deviation.

The water absorption and density of the prepared cement pastes were obtained from the three cubic specimens with dimensions of 3 × 3 × 3 cm^3 using the following expressions (Eqs. 1 and 2):

$$WaterAbsorption = \frac{W_S - W_D}{W_D} \cdot 100 \quad (1)$$

$$Density = \frac{m}{V} = \frac{W_D}{W_S - W_{WS}} \cdot \rho_w \quad (2)$$

Where, W_S is the weight of the sample saturated in water after removing excess water from the surface, W_D is the weight of the sample after 24 hours in an oven at 105°C, W_{WS} is the weight of the sample saturated and immersed in water and ρ_w is the water density [57,58].

The standard deviation for the density values were calculated from the measurement of three specimens.

The porosity of the pastes, as well as the pore size distribution, was obtained by mercury intrusion porosimetry (MIP), using a Micromeritics Autopore IV 9500 analyser. The analyses were carried out on a fragment of a 3×3 x 3 cm^3 cubic test specimen, previously submerged in isopropanol for 48 h to stop the hydration processes, and then dried in an oven at 40°C for 24 hours.

2.4. Radionuclides measurement

Two types of samples were measured: i) powder samples measured in a cylindrical polypropylene container with a diameter of 76.5 mm and height of 30 mm and ii) cement pastes as cubic prisms of 5x5x5 cm^3. Radon exhalation loses were minimised by sealing the cylindrical container with parafilm and impregnating the six sides of the quadrangular prisms with an epoxy resin. The epoxy resin used consisted of a mixture of two components ($C_{30}H_{43}O_7Cl$ and $C_{17}H_{30}ON_2$) in a ratio of 100:60. Once the epoxy resin hardened, it had an average thickness of 0.15 mm on each prism face. To ensure the secular equilibrium between ^{226}Ra and ^{222}Rn, 30 days passed between the sample preparation and the gamma measurement. Different coaxial HPGe detectors were used: 2 extended range (XtRa), 1 broad energy (BEGe) and 1 reverse electrode (REGe). The full energy peak efficiency of the four detectors was determined using the Montecarlo code LabSOCS [59,60] and the true coincidence summing corrections (TCS) was applied using the Peak-To-Total method of Genie 2000 [61].

The activity concentration of ^{226}Ra was determined both directly from the 186 keV photopeak and indirectly from the short half-life gamma-emitting progeny (^{214}Pb and ^{214}Bi). The interferences produced by ^{235}U in the 186 keV photopeak were removed by calculating the counts due to ^{235}U from the 63 keV photopeak of ^{234}Th [62,63]. Other radionuclides as ^{210}Pb, ^{228}Ra, ^{228}Th, and ^{40}K were also determined. The procedure for averaging samples, backgrounds and quality controls was accredited by ENAC based on the UNE-EN ISO/IEC 17025:2017 standard [64].

The activity concentration index (I_C) provides an estimate of the suitability of a given final building material to ensure that the annual external excess dose above the natural background is less than 1 mSv [20,65], and is defined as:

$$I_c = \frac{C_{^{226}Ra}}{300} + \frac{C_{^{232}Th}}{200} + \frac{C_{^{40}K}}{3000} \quad (3)$$

With $C_{^{226}Ra}$, $C_{^{232}Th}$ and $C_{^{40}K}$ the activity concentration of ^{226}Ra, ^{232}Th and ^{40}K in Bq kg^{-1}.

In addition, the Spanish regulation [66] defined the index I_D to be

Fig. 3. Example of the samples prepared with the different moulds for the 100–0–2 specimens.

applied in the case of materials used as coating or insulation, the expression of which is as follows:

$$I_D = \left[\left(281+16.3\rho d-0.0161(\rho d)^2\right)C_{Ra_{226}}+\left(319+18.5\rho d -0.0178(\rho d)^2\right)C_{Th_{232}}+\left(22.3+1.28\rho d-0.0014(\rho d)^2\right)C_{K_{40}}\right]\cdot 10^{-6}+0.19 \quad (4)$$

Being ρ the density in kg m^{-3} and d the thickness of the material in m.

The two indexes indicated in the regulations were calculated for the 1x10x10 cm^3 pastes prepared in this study. The reference level established in [66] will be met when the value of the indexes is less than 1.

2.5. Emanation factor, radon potential, exhalation rate, measurement and radon diffusion coefficient measurement

The methodology used to obtain the radon emanation factor, the radon potential and the radon exhalation rate is based on placing the problem material inside an accumulation volume [67–69]. The radon concentration in the volume over time has a known equation, which is a balance between the radon generated by the material and the radon that is lost by natural radon decay, the system leakage and the back-diffusion effect. By measuring the radon concentration in the volume of accumulation for an interval of time and fitting the data of radon concentration versus the measurement time using a known equation, the emanation factor, radon potential and exhalation rate can be calculated.

The emanation factor and radon potential were measured for the powder raw material of cement and fly ash and the exhalation rate was measured for all the final pastes made with the 1 × 10 x 10 cm^3 mould. Our experimental set-up consists of a polypropylene chamber of 2.4 L, which will be the accumulation volume, and a radon detector. Two different radon detectors were used, a RTM 1688–2 [70] and a RAD7 [71] (Fig. 4).

The methodology applied to obtain the radon diffusion coefficient is based on the ISO 11665–13 [45]. The main idea is to place the problem material between two chambers, one of which will be empty (“receiver container”) and another one will contain a radon source (“source container”), generating a radon flow between both chambers. From the measurements of radon concentration in both chambers the radon diffusion coefficient, *D*, can be calculated. This is done by solving the diffusion problem equations inside the material and the accumulation of radon in the receiver container for different values of *D*. These estimated measurements are then compared with the experimental measurements until the value that best fits the data is found. All the calculations are done though a procedure developed by [47].

As the exhalation rate, the diffusion coefficient was measured for all the final pastes prepared with the mould of 1 × 10 x 10 cm^3. The experimental set-up is shown in Fig. 5 and consists of two accumulation chambers of 2.4 L each, a perforated cover where the problem material is placed that fits between the two chambers, a radon source, and two radon detectors, a RTM 1688–2 [70] and a RAD7 [71].

3. Results and discussion

3.1. Mechanical performance, physical characteristics and microstructure of the pastes

The results of mechanical strength are shown in Fig. 6.

It can be observed that the mechanical strengths of all the pastes (Fig. 6) show an increase between 2 and 28 days, which was to be

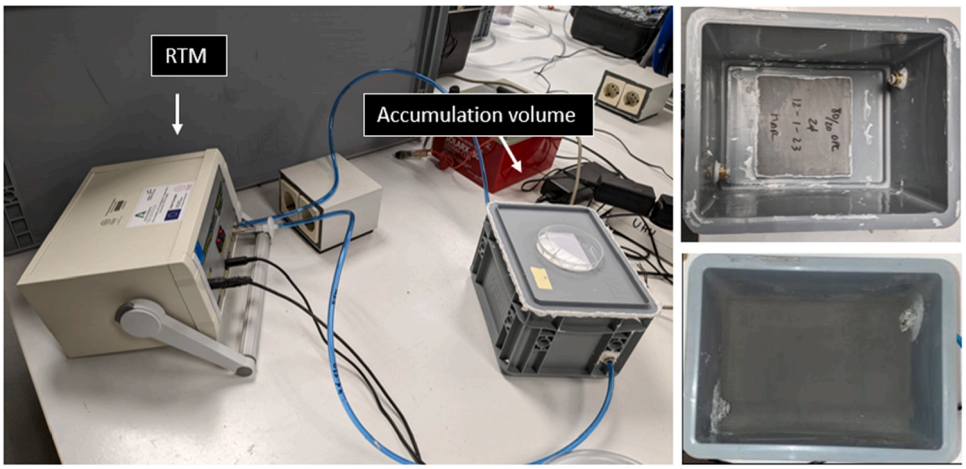

Fig. 4. Experimental set-up for the radon exhalation rate, radon emanation factor and radon potential measurements.

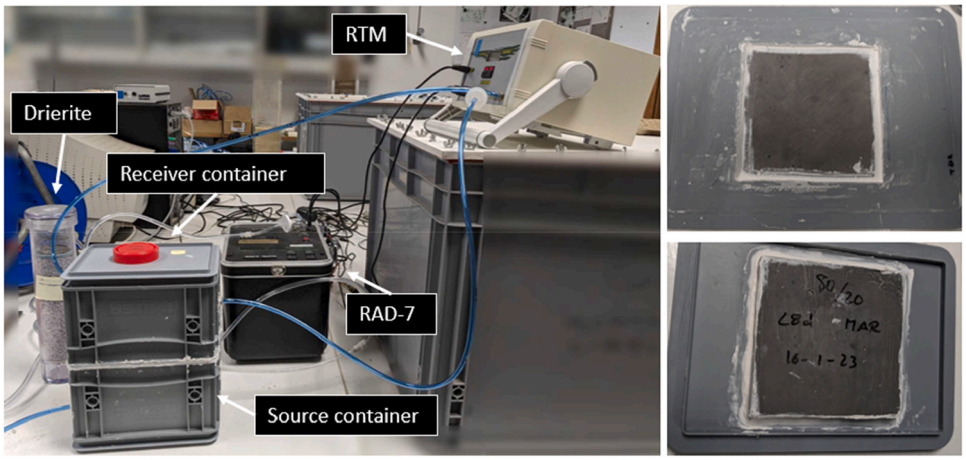

Fig. 5. Experimental set-up for the radon diffusion coefficient measurement.

expected due to the progress of hydration reactions. The substitution of CEM by different proportions of FA has a negative impact on the mechanical strength, higher as the percentage of substitution increases and more pronounced at 40% of replacement at 2 days. This effect is well known given that the pozzolanic reaction of FA is slow and at two days it has hardly occurred. At longer times (28 days) the negative effect of the replacement is becoming less pronounced [54].

However, the specimens prepared with superplasticiser admixture, which had a proportion of 30% FA, developed the highest compressive mechanical strengths at 2 and 28 days. Those that included 0.4% superplasticiser developed strengths of 68.2 and 112.6 MPa at ages 2 and 28 days, respectively. With the addition of 0.6% of superplasticiser, the tested specimens developed strengths of 69.0 and 113.6 MPa at curing ages of 2 and 28 days, respectively. No significant differences in mechanical strength results were observed between the samples prepared with 0.4% and those prepared with 0.6% admixture. The mechanical strength of the pastes with SP admixtures increased significantly as the admixture allows the reduction of the l/s ratio (see Table 3). This is due to the fact that the SP admixture deflocculates the cement particles, freeing the water retained between them, and thus improving the hydration of the pastes [72].

The water absorption and density of the hardened samples are shown in Fig. 7.

Regarding the pastes prepared without superplasticiser admixture, it can be observed that the water absorption in all the pastes (Fig. 7a) is higher at 2 days than at 28 days, as expected due to the progression of the hydration reactions at 28 days. The highest water absorption occurs in the 60–40–2 pastes with an increase of 14% compared to the pastes without FA.

The density values (Fig. 7b), follow the opposite trend as expected, and coherent with the water absorption values, presenting the lowest density for the 2-day sample with 40% substitution by FA (60−40−2).

The results for the porosity and pore size distribution of pastes are shown in Fig. 8.

The mercury porosimetry results (Fig. 8) show that in all cases, the 28-day pastes have lower values than the 2-day pastes, although no significant differences are observed in the pore size distribution.

All these results are perfectly coherent with the values obtained for the mechanical strengths (Fig. 6). The replacement of CEM by FA leads to a lower quantity of hydration products at early ages. The pozzolanic reaction of the FA with the portlandite resulting from the hydration of the CEM is a slower process and therefore, the higher the percentage of substitution, the lower the densification of the microstructure, the higher the porosity and therefore the higher the water absorption and the lower the mechanical strength, this effect being more evident at short ages [54,73]. In pastes with the addition of superplasticiser, and therefore with a lower w/c ratio, the densification of the samples increases, and the water absorption and porosity of the samples decreases considerably, being these effects more evident with 0.6% SP [74].

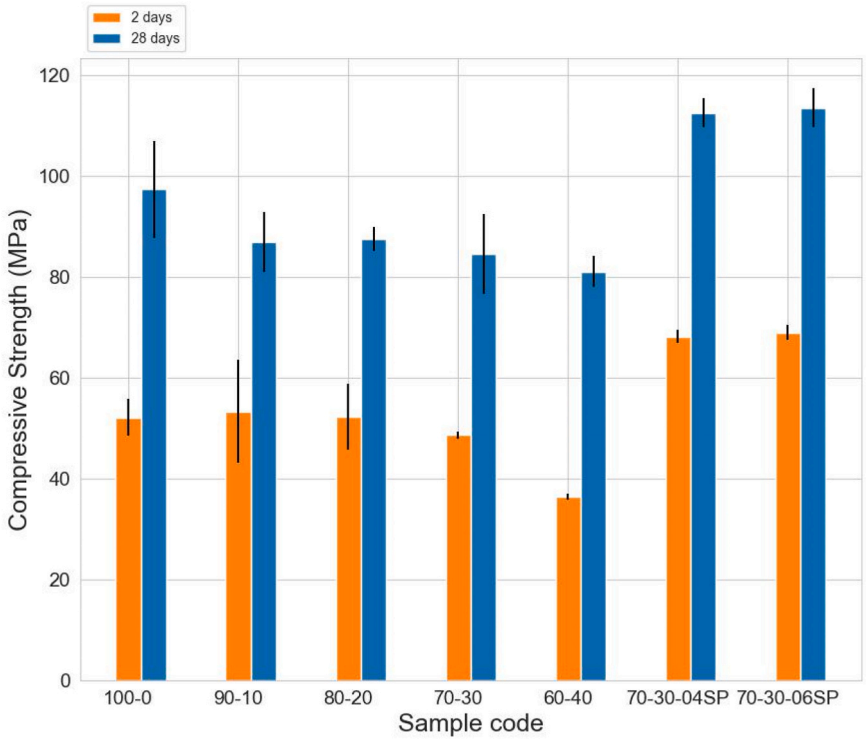

Fig. 6. Mechanical compressive strength of pastes as a function of their fly ash content and/or superplasticizer content.

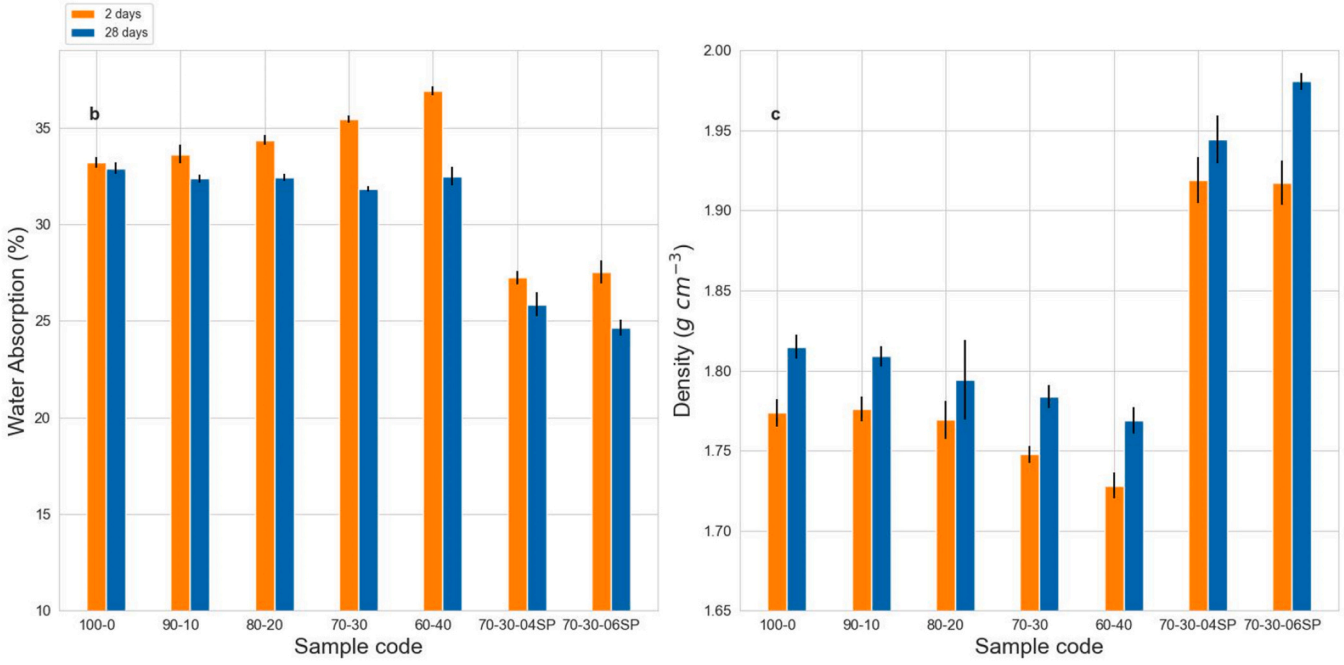

Fig. 7. a) Water absorption and b) density of pastes as a function of their fly ash content and/or superplasticizer content.

3.2. Radioactive characterization

3.2.1. Characterization of raw materials

Table 4 shows the activity concentrations obtained for the Portland cement (CEM) and fly ash (FA) as well as the activity ratios of $^{226}Ra/^{238}U$ and $^{210}Pb/^{226}Ra$.

The activity concentrations obtained for the reference cement and fly ash samples are similar to those determined in previous studies [75,76]. Also, for the cement, the activities are similar to those found on average in a typical Spanish soil [77,78]. For the FA, being a NORM material, there is an increase in the activity compared to the CEM. The fly ash came from the combustion of a coal with a high lignite content, which implies a higher activity concentration of radionuclides from the uranium series than from the thorium series [54].

Both the U-series and the Th-series radionuclides are in secular equilibrium in cements, as it is expected, excepting ^{210}Pb. This can be observed in the calculated activity ratios, being compatible with 1.

In the FA sample a significant disequilibrium ^{210}Pb-^{226}Ra is found.

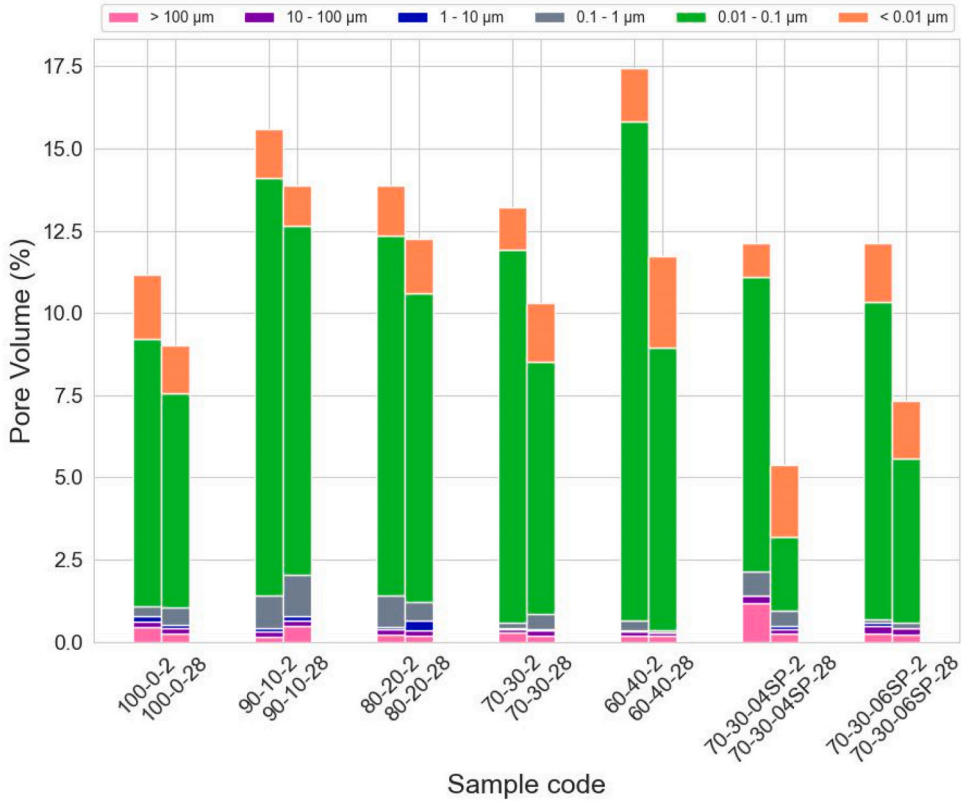

Fig. 8. Porosity and pore size distribution of pastes as a function of their fly ash content and/or superplasticizer content.

Table 4
Activity concentrations of the radionuclides of the natural radioactive series of uranium (^{234}Th, ^{214}Pb, ^{210}Pb) and thorium (^{228}Ac and ^{212}Pb) together with ^{40}K, and the ratios of the radionuclides of the radioactive series of uranium (^{226}Ra/^{238}U) and (^{210}Pb/^{226}Ra) for the Portland cement (CEM) and fly ash (FA).

	Activity concentration (Bq kg^{-1})								
	^{238}U-series			^{232}Th-series					
	^{238}U	^{226}Ra	^{210}Pb	^{228}Ra	^{228}Th	^{40}K	^{226}Ra/^{238}U	^{210}Pb/^{226}Ra	^{228}Th/^{228}Ra
CEM	33.1 ± 1.9	29.0 ± 1.0	24.9 ± 1.6	21.1 ± 0.6	22.5 ± 0.7	173 ± 8	0.88 ± 0.06	0.86 ± 0.06	1.07 ± 0.04
FA	167 ± 6	154 ± 7	105 ± 6	54.8 ± 1.7	55 ± 3	236 ± 6	0.92 ± 0.05	0.68 ± 0.05	1.00 ± 0.07

This fact is ratified by ^{210}Pb/^{226}Ra activity concentration ratio is less than 1, implying ^{210}Pb losses in relation to 226Ra, its parent and a refractory radionuclide not lost in combustion processes. The loss of ^{210}Pb is due to the range of temperatures reached in the furnace, between 1500 and 1600 °C, which causes ^{210}Pb to leave the burner in a gaseous state together with the flue gas [79,80].

Table 5
Activity concentrations of the radionuclides of the natural radioactive series of uranium (^{234}Th, ^{214}Pb, ^{210}Pb) and thorium (^{228}Ac and ^{212}Pb) together with ^{40}K, and the ratios of the radionuclides of the radioactive series of uranium (^{226}Ra/^{238}U) and (^{210}Pb/^{226}Ra) for the final pastes.

	Activity concentration (Bq kg^{-1})								
	^{238}U-series			^{232}Th-series					
	^{238}U	^{226}Ra	^{210}Pb	^{228}Ra	^{228}Th	^{40}K	^{226}Ra/^{238}U	^{210}Pb/^{226}Ra	^{228}Th/^{228}Ra
100–0–2	14.3 ± 2.0	16.6 ± 1.0	17 ± 3	15.9 ± 0.6	16.6 ± 1.0	158 ± 5	1.2 ± 0.4	1.0 ± 0.3	1.04 ± 0.07
100–0–28	18 ± 3	15.8 ± 1.0	17 ± 4	16.6 ± 0.6	16.0 ± 1.0	137 ± 4	0.9 ± 0.3	1.1 ± 0.5	1.03 ± 0.07
90–10–2	23 ± 3	27.0 ± 1.6	20 ± 4	18.8 ± 0.7	19.9 ± 1.2	156 ± 5	1.2 ± 0.4	0.7 ± 0.3	1.06 ± 0.07
90–10–28	29 ± 3	27.4 ± 1.6	22 ± 3	18.4 ± 0.6	19.2 ± 1.1	139 ± 4	0.95 ± 0.21	0.81 ± 0.25	1.05 ± 0.07
80–20–2	48 ± 4	41.1 ± 2.4	43 ± 4	23.6 ± 0.8	24.8 ± 1.5	178 ± 6	0.86 ± 0.18	1.05 ± 0.23	1.05 ± 0.07
80–20–28	46 ± 4	40.0 ± 2.2	35 ± 5	21.0 ± 0.6	22.9 ± 1.3	146 ± 5	0.87 ± 0.20	0.9 ± 0.3	1.09 ± 0.07
70–30–2	58 ± 5	50 ± 3	40 ± 5	26.0 ± 0.9	25.3 ± 1.4	164 ± 5	0.86 ± 0.19	0.80 ± 0.24	0.97 ± 0.06
70–30–28	69 ± 4	48 ± 3	46 ± 5	24.2 ± 0.8	25.5 ± 1.5	152 ± 5	0.70 ± 0.12	0.96 ± 0.22	1.05 ± 0.07
60–40–2	91 ± 5	70 ± 4	71 ± 5	30.7 ± 0.9	31.2 ± 1.8	177 ± 6	0.76 ± 0.13	1.02 ± 0.20	1.01 ± 0.07
60–40–28	86 ± 5	63 ± 4	60 ± 4	28.5 ± 1.0	30.2 ± 1.8	171 ± 6	0.73 ± 0.12	0.94 ± 0.18	1.06 ± 0.07
70–30–04SP−2	59 ± 5	51 ± 3	44 ± 5	26.2 ± 0.8	27.1 ± 1.6	162 ± 5	0.86 ± 0.18	0.86 ± 0.24	1.04 ± 0.07
70–30–04SP−28	61 ± 6	50 ± 3	44 ± 6	25.1 ± 0.8	25.9 ± 1.5	140.7 ± 5	0.82 ± 0.19	0.88 ± 0.24	1.03 ± 0.07
70–30–06SP−2	74 ± 5	54 ± 3	58 ± 6	27.2 ± 1.0	28.3 ± 1.7	178 ± 6	0.73 ± 0.14	1.07 ± 0.24	1.04 ± 0.07
70–30–06SP−28	66 ± 5	58 ± 3	60 ± 5	25.8 ± 0.8	28.2 ± 1.6	159 ± 5	0.89 ± 0.16	1.03 ± 0.22	1.09 ± 0.07

3.2.2. Activity concentration indices for gamma radiation

Table 5 shows the activity concentrations for the final products as well as the activity ratios of $^{226}Ra/^{238}U$ and $^{210}Pb/^{226}Ra$.

These results agree with those found in the literature [81]. The activity concentrations of natural radionuclides (Table 5) were compared with those calculated from the activity concentrations measured for the raw materials (CEM and FA) (Table 4) considering their ratios. The two-tailed paired samples Student's *t*-test was used in order to study if the activity concentrations were significantly different from each other [82]. The results showed that the ^{238}U, ^{226}Ra and ^{228}Th were statistically compatible, obtaining values of $p > 0.05$. For the ^{210}Pb a p-value of 0.012 was obtained, implying significant differences, however the reason for this difference is due to the high uncertainty in the determination of ^{210}Pb. Also, as the percentage of FA increases, the results for activity concentration increase, as would be expected from increasing the amount of a NORM material in the final paste.

The $^{226}Ra/^{238}U$ ratio in Table 5 would indicate that there could be losses of ^{222}Rn through the vertices of the cubic prism. This behaviour was not observed in the case of the $^{210}Pb/^{226}Ra$ ratio in which, although the FA showed an imbalance, most of the values were close to 1 since its percentage is low in the cubes, minimising this effect and being, in many cases, included in the uncertainty. Finally, for the $^{228}Th/^{228}Ra$ equilibrium factor, the results were compatible with 1.

Fig. 9 shows the indices for gamma radiation I_C and I_D for the final pastes.

The secular equilibrium between ^{228}Ra and ^{232}Th was assumed due to the fact that in the thermal process both the radio and the thorium are very refractory and the secular equilibrium present in the raw materials is not broken [83–88]. The gamma radiation index I_C and I_D, for all the final materials, are less than 1, which is the reference value established. This means that these materials are suitable for their use in construction, in terms of their gamma activity, and as a coating or insulation against radon. Also, as expected, both indices increase with increasing FA (Fig. 9), as the activity concentrations of ^{226}Ra, ^{232}Th and ^{40}K increase with the percentage of FA (Table 5).

3.3. Exhalation rate, emanation factor, radon potential measurement and radon diffusion coefficient measurement

The results for the emanation factor and the radon potential of the raw materials, CEM and FA, are shown in Table 6.

The values obtained are comparable with those found in the literature [89,90], both for the CEM and the FA. The emanation factor for the FA is lower than for the CEM. However, the radon potential is higher for the FA than for the CEM for the higher activity concentration of the FA, meaning that the potential radiological risk of the material is higher, as the radon potential represents the radon activity generated inside the material that has the potential to be transported though the material to the surrounding atmosphere.

For the 14 pastes, the radon exhalation rate, *E*, was measured and is shown in Table 7.

The values found in the literature for the exhalation of radon from cement pastes with fly ash vary, but our results are in the value range of those found [91–93]. They are also lower than the typical soil average of 57.6 Bq m^{-2} h^{-1} [94,95], as our final pastes are hardened materials that develop a microstructure that make the materials denser.

When the radon exhaled by the samples was calculated, in some cases it was difficult to reduce the uncertainty of the measurements in order to obtain a good fit of the data, as can be seen in Fig. 10 for sample 70–30–06SP-28 which has the highest relative uncertainty for the radon exhalation rates results. Even when using a measurement cycle of 4 hours concentrations with hight uncertainty values were measured, giving exhalation values with a high uncertainty and not very clear trends in the results with composition or with curing days.

The results are also represented in Fig. 11 versus some pastes properties. In Fig. 11a the *E* is plotted on the percentage of fly ash only for the samples without plasticiser additive. For the samples with a 70% of

Table 6
Radon emanation factor and radon potential of CEM and FA.

	Emanation factor (%)	Radon potential (Bq kg^{-1})
CEM	12 ± 3	3.5 ± 1.0
FA	3.5 ± 0.6	5.4 ± 1.0

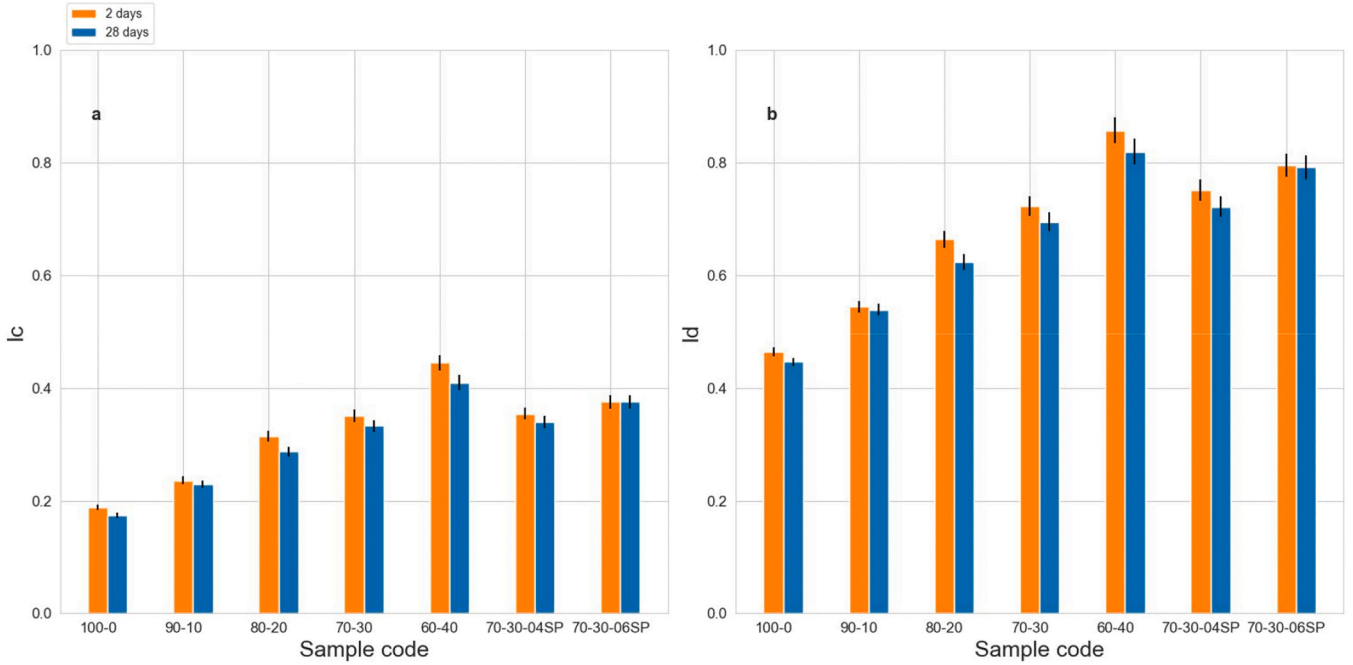

Fig. 9. Activity concentration index a) I_C and b) I_D for the final pastes as a function of their fly ash content and/or superplasticizer content.

Table 7
Radon exhalation rate for the final pastes.

Code	E (Bq m^{-2} h^{-1})
100–0–2	0.83 ± 0.13
100–0–28	0.41 ± 0.10
90–10–2	1.01 ± 0.13
90–10–28	0.92 ± 0.21
80–20–2	1.35 ± 0.18
80–20–28	2.9 ± 0.5
70–30–2	1.3 ± 0.3
70–30–28	1.5 ± 0.3
60–40–2	1.5 ± 0.6
60–40–28	2.5 ± 0.7
70–30–04SP–2	2.1 ± 0.7
70–30–04SP–28	0.84 ± 0.14
70–30–06SP–2	1.05 ± 0.23
70–30–06SP–28	0.8 ± 0.5

cement, 30% of fly ash and different additions of superplasticiser the results are shown in Fig. 11b as a function of the percentage of admixture.

For the 2-days samples, there is a slight increase with the percentage of flying ash (Fig. 11a). This increase is higher for the samples with 28 days of curing, although the tendency is not always the same as we increase the fly ash percentage, with a decrease in the result going from a 20% to a 30%. In the case of the samples with 70% of cement and 30% fly ash, there is a slight decrease for the 28-days cured samples and no tendency for the samples with 2 days of curing (Fig. 11b).

The radon diffusion coefficient, *D*, of the 14 samples was calculated and the results are presented in Table 8 together with the sample code.

The range of values for Portland cement pastes with different admixtures found in the literature goes from $5.8\bullet10^{-10}$ m^2 s^{-1} to $420\bullet10^{-10}$ m^2 s^{-1} [96–98], being some on our results lower than these values. At least two measurements for sample were made in order to calculate a mean value and an uncertainty with the standard deviation of the mean, and the results obtain were always similar values with the same order of magnitude, showing the consistency of the methodology.

The results are also shown in Fig. 12, represented in a way that only one variable is being changed at a time. In Fig. 12a the *D* of samples without plasticiser additive is represented as a function of the percentage of flying ash. The *D* of the samples with a 70% of cement, 30% of flying ash and different additions of plasticiser is shown in Fig. 12b as a function of the percentage of additive. In both cases, the results are separated by their curing time in two different lines.

Looking at Fig. 12, it is clear that for the samples with the same composition, i.e. the same percentage of cement, fly ash and additive, there is a dependence of *D* with the curing time, being the materials with a longer curing time systematically less permeable. This change in the permeability reaches in some cases higher than a factor of 10, from $2.9\bullet10^{-10}$ m^2 s^{-1} in sample 60–40–28 to $6.65\bullet10^{-9}$ m^2 s^{-1} in sample 60–40–2, which can be an important factor to consider when the material is used as a radon barrier. Without the plasticiser additive (Fig. 12a), the order of magnitude is of 10^{-10} m^2 s^{-1} for the 28-day curing time samples and of 10^{-9} m^2 s^{-1} for the 2-day curing time samples. For the samples with a curing time of 28 days, there is a slight increase in *D* with increasing fly ash content. For the samples with a curing time of 2 days, there is no clear dependence.

All these results are consistent with those obtained for the density, porosity and water absorption of the samples (Fig. 6). The samples with a 28-day curing time have a lower porosity, which results in less available path for radon and a lower *D* value. There is also an increase in density between the samples with a 28-day curing time and the 2-day curing time, which has also been found to have an inverse relationship with *D* [98,99]. The higher the densification of the microstructure, the lower the pore volume and therefore the lower the diffusion *D*.

When a superplasticiser admixture is added for the same percentage of cement and fly ash, 70% and 30% respectively, (Fig. 12b), the lower curing time samples still have a higher *D*. There is also a more pronounced change in *D* with the percentage of plasticiser additive than with fly ash, even in order of magnitude, decreasing as the percentage of admixture increases.

This is due to the lower w/c ratio used in the admixture samples which leads to much higher densification and a very sharp decrease in

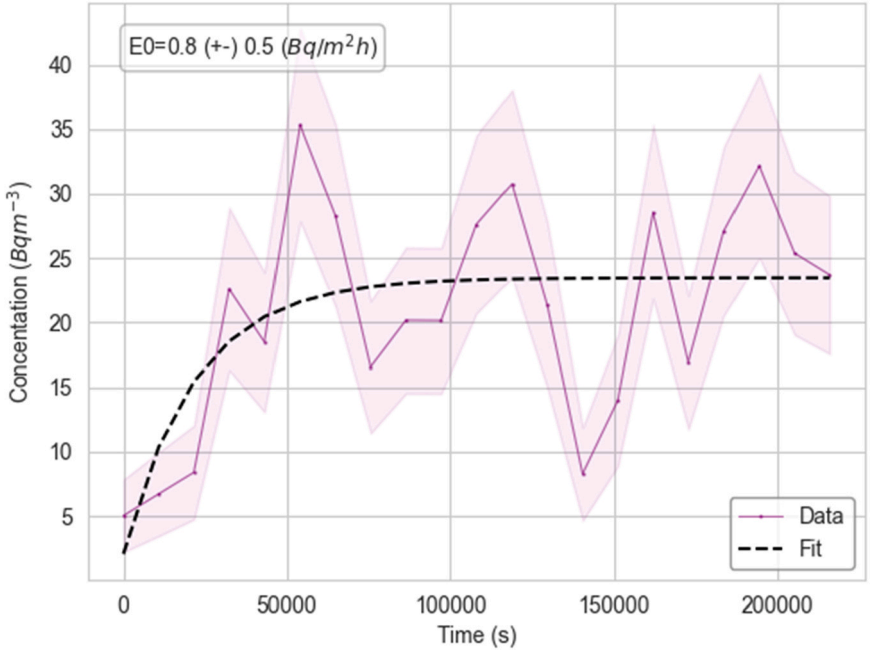

Fig. 10. Radon concentration measurements for the 70–30–06SP-28 sample used to calculate the radon exhalation rate.

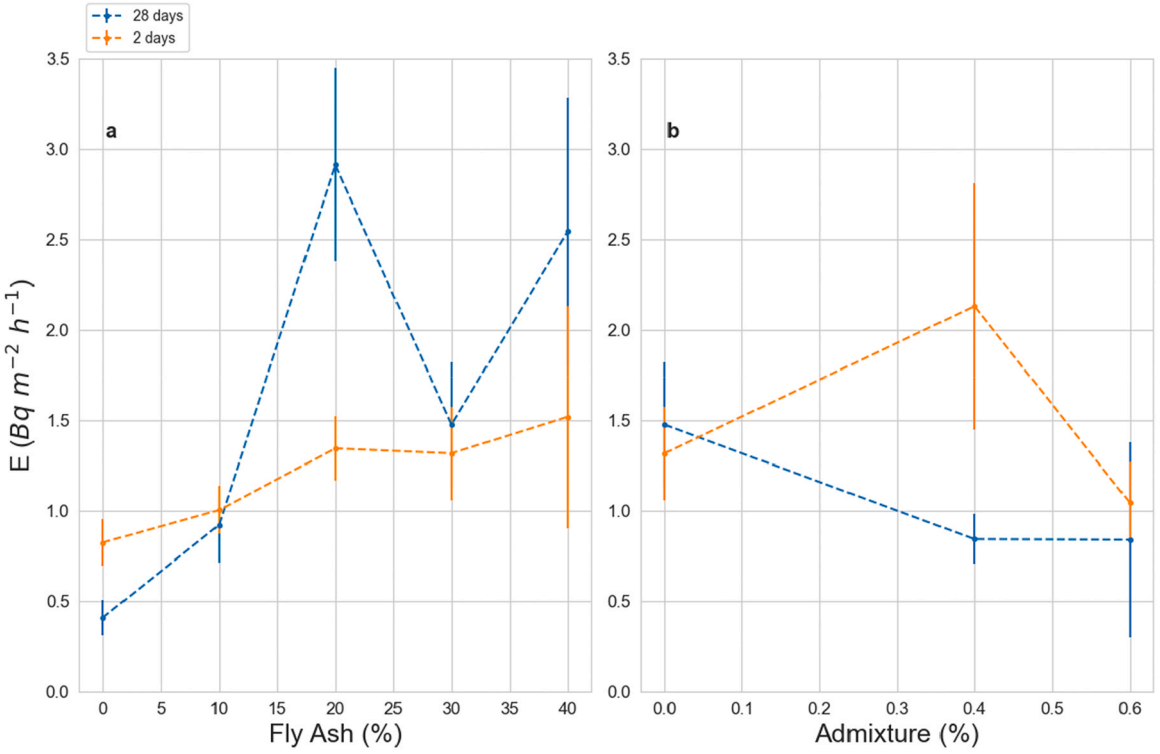

Fig. 11. Radon exhalation rate, E, a) varying the percentage of fly ash and b) varying the percentage of superplasticizer admixture, fixing the percentage of cement and fly ash at 70% and 30%, respectively, for this latter case. The curing time was fixed at 2 days and 28 days.

Table 8
Radon diffusion coefficient for the final pastes.

Code	D (m^2 s^{-1}) $\cdot 10^{-10}$
100–0–2	49.8 ± 0.3
100–0–28	1.2 ± 0.3
90–10–2	17.7 ± 0.3
90–10–28	1.2 ± 0.4
80–20–2	28.4 ± 0.6
80–20–28	1.38 ± 0.08
70–30–2	18.47 ± 0.15
70–30–28	2.8 ± 0.3
60–40–2	66.5 ± 1.8
60–40–28	2.9 ± 0.3
70–30–04SP−2	3.86 ± 0.11
70–30–04SP−28	1.09 ± 0.09
70–30–06SP−2	1.15 ± 0.20
70–30–06SP−28	0.43 ± 0.04

the porosity of the samples more pronounced for the 28-day curing time samples, and an increase in the density. These changes in the microstructure of the pastes could be the cause of the decrease in *D*. (Table 3 and Fig. 6). In other words, the use of a small percentage of superplasticiser can make the final material less permeable to radon by up to an order of magnitude, making it an interesting topic to consider when reducing the diffusion of radon gas from the soil at building foundations.

Also, looking at Fig. 12b, the reduction of the radon diffusion coefficient with the higher curing days is lesser for the samples with superplasticiser admixture. This could be caused by the lower w/c ratios for those samples, and the reduction in porosity even for early ages (2 days curing time). The decrease in porosity observed in other pastes between 2 and 28 days is therefore not so evident in pastes with superplasticiser. Therefore, the difference between the radon diffusion coefficient values between 2 and 28 days in pastes with superplasticiser is also smaller.

The lowest *D* measured was for the sample 70–30–06SP-28, which was (4.3 ± 0.4) •10^{-11} m^2 s^{-1}, having the advantage of reducing *D* for his higher curing time and the presence of the admixtures. To better illustrate these findings in Fig. 13 the density and *D* of the samples are plotted together.

For both cases, the 2 day (Fig. 13a) and 28 day (Fig. 13b) curing time samples, it is clear that there is an inverse relationship between the two variables. From these results it can be concluded that building materials containing NORM materials in their composition, can be used as radon insulating materials and decrease their permeability to radon, if the appropriate microstructure is developed

4. Conclusions

The radon diffusion coefficient, *D*, and the radon exhalation rate, *E*, of 7 types of Portland Cement pastes, with different percentages of fly ash and superplasticiser admixtures, were measured, together with a study of their mechanical properties and a radioactive characterisation. This was done in order to gain a better understanding of which characteristics influence the final radon properties of the materials, and to investigate the possibility of using a cement paste as an insulation material against radon in buildings.

The main results were that the *D* of the pastes with a higher number of curing days and a higher percentage of superplasticiser admixture were found to be lower, i.e., the pastes were less permeable to radon. This was due to the correlation between the mechanical properties of the pastes and the diffusion, as a higher densification of the paste results in a lower porosity and ultimately a lower *D*, as there is less path available for the radon gas to diffuse. This is due to the progress of hydration by

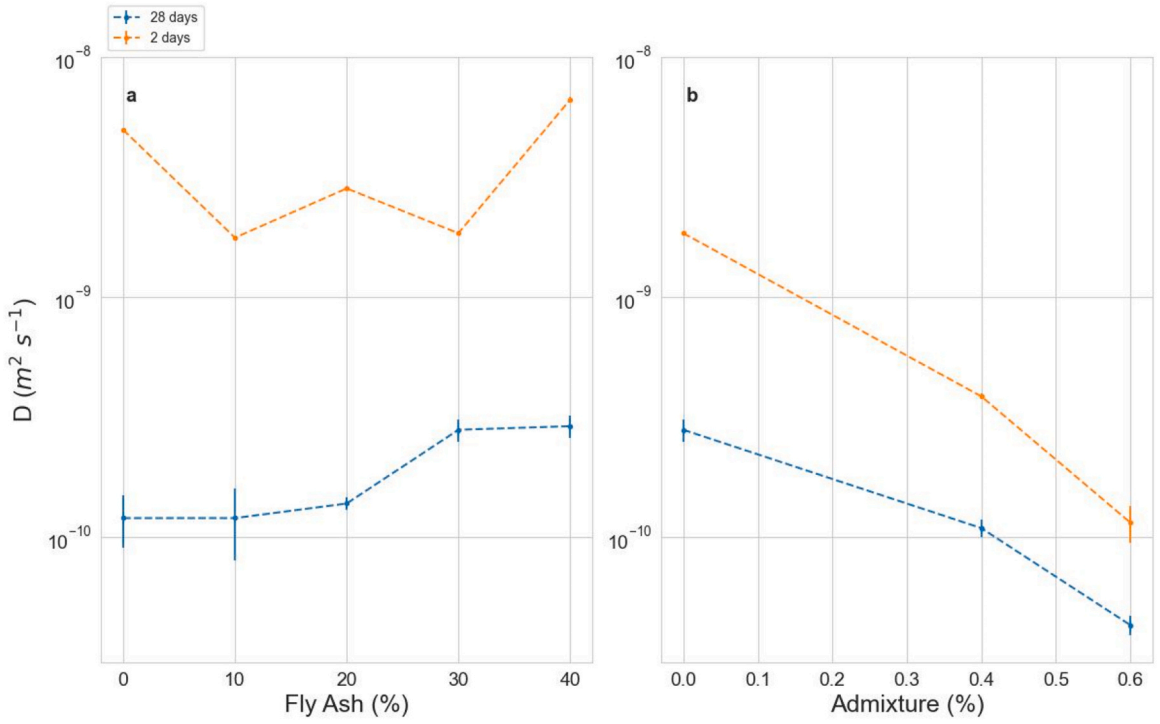

Fig. 12. Radon diffusion coefficient, D, a) varying the percentage of fly ash and b) varying the percentage of superplasticiser admixture, fixing the percentage of cement and fly ash at 70% and 30%, respectively, for this latter case. The curing time was fixed at 2 days and 28 days. The scale for the y-axis is logarithmic.

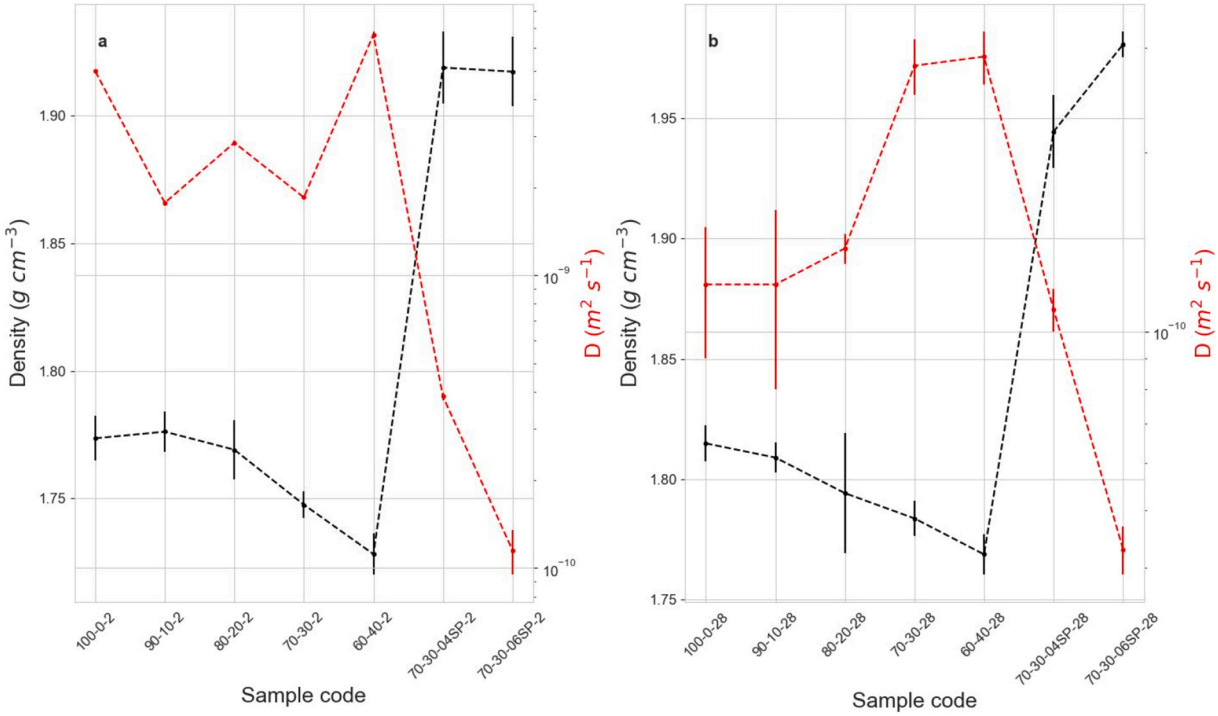

Fig. 13. Density and Radon diffusion coefficient, D, in different pastes at a) 2 days curing time and b) 28 day curing time.

chemical reaction with higher curing days and the improvement of hydration by the deflocculation caused by the SP admixture.

In conclusion, the development of a low porosity samples due to a higher number of curing days and the addition of superplasticiser admixture can produce a paste which, although containing a NORM material, has a very low radon permeability and is a good insulating material.

CRediT authorship contribution statement

E. Castaño-Casco: Methodology, Formal analysis, Investigation, Data curation, Writing – original draft, Writing – Review & Editing. **A. Caño:** Methodology, Formal analysis, Investigation, Data curation, Writing – original draft, Writing – Review & Editing. **J.A. Suárez-Navarro:** Conceptualization, Methodology, Formal analysis, Investigation, Data curation, Writing – original draft, Writing – Review & Editing, Supervision, Project Administration. **I. Gutiérrez-Álvarez:** Methodology, Formal analysis, Investigation, Data curation, Writing – Review & Editing. **A. Barba-Lobo:** Methodology, Formal analysis, Investigation, Data curation, Writing – Review & Editing. **J.P. Bolívar:** Conceptualization, Methodology, Formal analysis, Investigation, Resources, Data curation, Writing – Review & Editing, Supervision, Project Administration, Funding acquisition. **M.M. Alonso:** Conceptualization, Methodology, Formal analysis, Investigation, Resources, Data curation, Writing – original draft, Writing – Review & Editing, Supervision, Project Administration, Funding acquisition.

Declaration of Competing Interest

The authors declare that they have no known competing financial interests or personal relationships that could have appeared to influence the work reported in this paper.

Acknowledgements

This research was partially funded by different projects: the project funded by the Nuclear Safety Council (CSN) “Radon exhalation from building materials; Radiological impact and corrective measures (EXRADON)” (PR-047-2021), by grant PID2020-116461RB-C21 (RAD-REMOVE) funded by MICIU/AEI/10.13039/501100011033, by grant TED2021-130361B–I00 (RESTOREHU) funded by MICIU/AEI/10.13039/501100011033, as finally by research Project PID2020-116002RB-100/AEI/10.13039/501100011033 (HORRADIONEX) supported the Spanish Ministry of Science and Innovation, the Spanish National Research Agency (AEI).

The authors would also like to thank the MICIM for the pre-doctoral contract (PRE2021-098535) of Andrés Caño Blanes. We also thank Queralt Belen Marzal for her help in laboratory tests.

Data availability

Data will be made available on request.

References

[1] UNEP, Disclaimers Suggested citation Production Penrose CDB, 2022. ⟨www.globalabc.org⟩.
[2] M. Hanifa, R. Agarwal, U. Sharma, P.C. Thapliyal, L.P. Singh, A review on CO2 capture and sequestration in the construction industry: emerging approaches and commercialised technologies, J. CO2 Util. 67 (2023) 102292, https://doi.org/10.1016/j.jcou.2022.102292.
[3] Z. Xue, W. Zhu, L. Li, C. Jiang, C. Yan, Y. Wang, J. Gao, J. Luo, Carbon emissions assessment of cement mixing piles for soft loess improvement and carbon emission reduction using white mud-cement composite material, Case Stud. Constr. Mater. 21 (2024) e03397, https://doi.org/10.1016/j.cscm.2024.e03397.
[4] M. Sandanayake, D. Law, P. Sargent, A new framework for assessing the environmental impacts of circular economy friendly soil waste-based geopolymer cements, Build. Environ. 210 (2022) 108702, https://doi.org/10.1016/j.buildenv.2021.108702.
[5] A.A. Al-Rawas, A. Wahid Hago, R. Taha, K. Al-Kharousi, Use of incinerator ash as a replacement for cement and sand in cement mortars, Build. Environ. 40 (2005) 1261–1266, https://doi.org/10.1016/j.buildenv.2004.10.009.
[6] R. Snellings, P. Suraneni, J. Skibsted, Future and emerging supplementary cementitious materials, Cem. Concr. Res 171 (2023) 107199, https://doi.org/10.1016/j.cemconres.2023.107199.
[7] Y. Wang, X. Hu, Q. Pei, X. Cui, P. Qi, Z. Xue, Improvement of mechanical behavior of cemented soil reinforced with waste sisal fibers: an optimal selection and modification research, Case Stud. Constr. Mater. 21 (2024) e03515, https://doi.org/10.1016/j.cscm.2024.e03515.
[8] CEN, EN 197-1:2011 Cement - Part 1: Composition, specifications and conformity criteria for common cements, 2011.
[9] F. Puertas, J.A. Suárez-Navarro, M.M. Alonso, C. Gascó, NORM waste, cements, and concretes. A review, Mater. De. Construcci. 71 (2021) e259, https://doi.org/10.3989/mc.2021.13520.
[10] R.P. Costa, M.H.G. de Medeiros, E.D. Rodriguez Martinez, V.A. Quarcioni, S. Suzuki, A.P. Kirchheim, Effect of soluble phosphate, fluoride, and pH in Brazilian phosphogypsum used as setting retarder on Portland cement hydration, Case Stud. Constr. Mater. 17 (2022) e01413, https://doi.org/10.1016/j.cscm.2022.e01413.
[11] C. Di Carlo, A. Maiorana, M. Ampollini, S. Antignani, M. Caprio, C. Carpentieri, F. Bochicchio, Models of radon exhalation from building structures: general and case-specific solutions, Sci. Total Environ. 885 (2023), https://doi.org/10.1016/j.scitotenv.2023.163800.
[12] J. Porstendorfer, G. Buttenveck, A. Reineking, Daily variation of the radon concentration indoors and outdoors and the influence of meteorological parameters, Note (1994).
[13] F. Pacheco-Torgal, Indoor radon: an overview on a perennial problem, Build. Environ. 58 (2012) 270–277, https://doi.org/10.1016/j.buildenv.2012.08.004.
[14] P. Sahu, D.C. Panigrahi, D.P. Mishra, Sources of radon and its measurement techniques in underground uranium mines – an overview, J. Sustain. Min. 13 (2014) 11–18, https://doi.org/10.7424/jsm140303.
[15] S. Darby, D. Hill, A. Auvinen, J.M. Barros-Dios, H. Baysson, F. Bochicchio, H. Deo, R. Falk, F. Forastiere, M. Hakama, I. Heid, L. Kreienbrock, M. Kreuzer, F. Lagarde, I. Mäkeläinen, C. Muirhead, W. Oberaigner, G. Pershagen, A. Ruano-Ravina, E. Ruosteenoja, A.Schaffrath Rosario, M. Tirmarche, L. Tomášek, E. Whitley, H. E. Wichmann, R. Doll, Radon in homes and risk of lung cancer: collaborative analysis of individual data from 13 European case-control studies, Br. Med. J. 330 (2005) 223–226, https://doi.org/10.1136/bmj.38308.477650.63.
[16] UNSCEAR, Sources and effects of ionizing radiation: United Nations Scientific Committee on the Effects of Atomic Radiation: UNSCEAR 2008 report to the General Assembly, with scientific annexes., United Nations, 2008. ⟨https://www.unscear.org/⟩ (accessed January 25, 2024).
[17] UNSCEAR, Report to the General Assembly SCIENTIFIC ANNEXES A and B, 2019. ⟨https://www.unscear.org/⟩ (accessed January 25, 2024).
[18] ICRP, Summary of ICRP recommendations on radon, 2018. ⟨https://www.icrp.org/⟩ (accessed January 25, 2024).
[19] WHO, WHO handbook on indoor radon: a public health perspective, World Health Organization, 2009.
[20] EURATOM, Directiva 2013/59/Euratom del Consejo, de 5 de diciembre de 2013, por la que se establecen normas de seguridad básicas para la protección contra los peligros derivados de la exposición a radiaciones ionizantes, y se derogan las Directivas 89/618/Euratom, 90/641/Euratom, 96/29/Euratom, 97/43/Euratom y 2003/122/Euratom, 2013. ⟨https://www.boe.es/⟩ (accessed January 25, 2024).
[21] BOE, Real Decreto 732/2019, de 20 de diciembre, por el que se modifica el Código Técnico de la Edificación, aprobado por el Real Decreto 314/2006, de 17 de marzo., 2019. ⟨https://www.boe.es⟩.
[22] R.C. Bruno, Sources of indoor radon in houses: a review, J. Air Pollut. Control Assoc. 33 (1983) 105–109, https://doi.org/10.1080/00022470.1983.10465550.
[23] C. Di Carlo, M. Ampollini, S. Antignani, M. Caprio, C. Carpentieri, B. Caccia, F. Bochicchio, Extreme reverse seasonal variations of indoor radon concentration and possible implications on some measurement protocols and remedial strategies, Environ. Pollut. 327 (2023), https://doi.org/10.1016/j.envpol.2023.121480.
[24] J.C.H. Miles, Temporal variation of radon levels in houses and implications for radon measurement strategies, Radiat. Prot. Dosim. 93 (2001) 369–375, https://doi.org/10.1093/oxfordjournals.rpd.a006449.
[25] B. Collignan, C. Lorkowski, R. Améon, Development of a methodology to characterize radon entry in dwellings, Build. Environ. 57 (2012) 176–183, https://doi.org/10.1016/j.buildenv.2012.05.002.
[26] IAEA, Protection of the public against exposure indoors due to radon and other natural sources of radiation, 2015. ⟨http://www-ns.iaea.org/standards/⟩.
[27] B.A. Moed, W.W. Nazaroff, Soil as a Source of Indoor Radon: Generation, Migration, and Entry, in: Radon and Its Decay Products in Indoor Air, 1988.
[28] A. Tsapalov, K. Kovler, Control of radon emanation at determination of activity concentration index for building materials, Constr. Build. Mater. 160 (2018) 810–817, https://doi.org/10.1016/j.conbuildmat.2017.11.116.
[29] C. Sabbarese, F. Ambrosino, A. D'Onofrio, V. Roca, Radiological characterization of natural building materials from the Campania region (Southern Italy), Constr. Build. Mater. 268 (2021), https://doi.org/10.1016/j.conbuildmat.2020.121087.
[30] P. Bossew, The radon emanation power of building materials, soils and rocks, Appl. Radiat. Isot. 59 (2003) 389–392, https://doi.org/10.1016/j.apradiso.2003.07.001.
[31] P. Gopalakrishnan, J. Jeyanthi, Importance of radon assessment in indoor Environment-a review, Mater. Today Proc. 56 (2022) 1495–1500, https://doi.org/10.1016/j.matpr.2021.12.534.
[32] R.M. Harrison, R.E. Hester, Indoor Air Pollution, The Royal Society of Chemistry, 2019, https://doi.org/10.1039/9781788016179.
[33] M. Jiranek, M. Kotrbata, Radon diffusion coefficients in 360 waterproof materials of different chemical composition, Radiat. Prot. Dosim. 145 (2011) 178–183, https://doi.org/10.1093/rpd/ncr043.
[34] M. Jiránek, V. Kačmaříková, Radon diffusion coefficients and radon resistances of waterproofing materials available on the building market, J. Environ. Radio. 208–209 (2019), https://doi.org/10.1016/j.jenvrad.2019.106019.
[35] B. Ruvira, B. García-Fayos, B. Juste, J.M. Arnal, G. Verdú, Experimental estimation of the diffusion coefficient in radon barrier materials based on ISO/TS 11665-13: 2017, Radiat. Phys. Chem. 193 (2022), https://doi.org/10.1016/j.radphyschem.2022.109993.

[36] B. Ruvira, B. García-Fayos, B. Juste, J.M. Arnal, G. Verdú, Determination of the radon diffusion coefficient of thin polyethene and aluminium foils used as single or multilayer configuration barriers, Radiat. Phys. Chem. 200 (2022), https://doi.org/10.1016/j.radphyschem.2022.110329.
[37] A. Tsapalov, K. Kovler, Revisiting the concept for evaluation of radon protective properties of building insulation materials, Build. Environ. 95 (2016) 182–188, https://doi.org/10.1016/j.buildenv.2015.09.020.
[38] K. Rovenská, M. Jiránek, Radon diffusion coefficient measurement in waterproofings - a review of methods and an analysis of differences in results, Appl. Radiat. Isot. 70 (2012) 802–807, https://doi.org/10.1016/j.apradiso.2012.01.002.
[39] W. Arafa, Permeability of radon-222 through some materials, Radiat. Meas. 35 (2002) 207–211, https://doi.org/10.1016/S1350-4487(02)00043-4.
[40] L.S. Quindos, A method for measuring effective radon diffusion coefficients in radon barriers by using modified Lucas cells, Radiat. Meas. 39 (2005) 87–89, https://doi.org/10.1016/j.radmeas.2004.03.029.
[41] A. Tsapalov, L. Gulabyants, M. Livshits, K. Kovler, New method and installation for rapid determination of radon diffusion coefficient in various materials, J. Environ. Radio. 130 (2014) 7–14, https://doi.org/10.1016/j.jenvrad.2013.12.010.
[42] I. Cozmuta, E.R. Van Der Graaf, Methods for measuring diffusion coefficients of radon in building materials, Sci. Total Environ. 272 (2001) 323335, https://doi.org/10.1016/S0048-9697(01)00711-2.
[43] Y. jun Ye, W. hao Wu, S. yang Feng, C. huang Huang, S. Li, Simultaneous determination of the radon diffusion coefficient and the free radon production rate from compact porous emanation media, Build. Environ. 144 (2018) 66–71, https://doi.org/10.1016/j.buildenv.2018.08.015.
[44] S. yang Feng, H. qing Wang, Y. Cui, Y. jun Ye, X. yang Li, D. Xie, Z. zhong He, R. Yang, Monte Carlo method for determining radon diffusion coefficients in porous media, Radiat. Meas. 126 (2019), https://doi.org/10.1016/j.radmeas.2019.106130.
[45] ISO, Measurement of radioactivity in the environment-Air: radon 222-Part 13: Determination of the diffusion coefficient in waterproof materials: membrane two-side activity concentration test method, 2017. ⟨www.iso.org⟩.
[46] M. Jiranek, Z. Svoboda, Transient radon diffusion through radon-proof membranes: a new technique for more precise determination of the radon diffusion coefficient, Build. Environ. 44 (2009) 1318–1327, https://doi.org/10.1016/j.buildenv.2008.09.017.
[47] E. Castaño-Casco, I. Gutiérrez-Álvarez, A. Barba-Lobo, J.P. Bolívar, Development of a robust and precise methodology for the measurement of the radon diffusion coefficient in diverse materials, Constr. Build. Mater. 440 (2024) 137402, https://doi.org/10.1016/j.conbuildmat.2024.137402.
[48] IAEA, Protection of the public against exposure indoors due to radon and other natural sources of radiation, 2015. ⟨http://www-ns.iaea.org/standards/⟩.
[49] Environmental Protection Agency, Technical Guidance Document C Site Preparation and Resistance to Moisture, 2004.
[50] Federal Law Gazette, Radiation Protection Ordinance, 2018.
[51] Czech Standardization Agency, Czech Technical Standard CSN 73 0601 Protection of Buildings against Radon from the Soil, 2019.
[52] K. Kovler, Legislative aspects of radiation hazards from both gamma emitters and radon exhalation of concrete containing coal fly ash, Constr. Build. Mater. 25 (2011) 3404–3409, https://doi.org/10.1016/j.conbuildmat.2011.03.031.
[53] K. Kovler, A. Perevalov, V. Steiner, L.A. Metzger, Radon exhalation of cementitious materials made with coal fly ash: part 1 – scientific background and testing of the cement and fly ash emanation, J. Environ. Radio. 82 (2005) 321–334, https://doi.org/10.1016/j.jenvrad.2005.02.004.
[54] A.M. Moreno de los Reyes, J.A. Suárez-Navarro, M. del M. Alonso, C. Gascó, I. Sobrados, F. Puertas, New approach for the determination of radiological parameters on hardened cement pastes with coal fly ash, Materials 14 (2021) 475, https://doi.org/10.3390/ma14030475.
[55] A. Caño, J.A. Suárez-Navarro, F. Puertas, A. Fernández-Jiménez, M. del M. Alonso, New approach to determine the activity concentration index in cements, fly ashes, and slags on the basis of their chemical composition, Materials 16 (2023) 2677, https://doi.org/10.3390/ma16072677.
[56] UNE, UNE-EN 196-3:2017 Methods of testing cement - Part 3: Determination of setting times and soundness, 2017.
[57] UNE, UNE-EN 12390-7:2020; Testing Hardened Concrete—Part 7: Density of Hardened Concrete, AENOR, Madrid, Spain, 2021.
[58] UNE, UNE 83980:2014. In Concrete Durability. Test Methods. Determination of the Water Absorption, Density and Accessible Porosity for Water in Concrete; UNE: Madrid, Spain, (2014).
[59] A. Barba-Lobo, V.M. Expósito-Suárez, J.A. Suárez-Navarro, J.P. Bolívar, Robustness of LabSOCS calculating Ge detector efficiency for the measurement of radionuclides, Radiat. Phys. Chem. 205 (2023), https://doi.org/10.1016/j.radphyschem.2022.110734.
[60] J.A. Suárez-Navarro, A.M. Moreno-Reyes, C. Gascó, M.M. Alonso, F. Puertas, Gamma spectrometry and LabSOCS-calculated efficiency in the radiological characterisation of quadrangular and cubic specimens of hardened portland cement paste, Radiat. Phys. Chem. 171 (2020), https://doi.org/10.1016/j.radphyschem.2020.108709.
[61] Mirion Technologies, Coincidence Summing Library (Nuclides and lines), Canberra Industries, Inc., Meriden, 2008.
[62] J.A. Suárez-Navarro, J.F. Benavente, V.M. Expósito-Suárez, A. Caño, G. Hernaiz, M. M. Alonso, 226Ra activity concentration determined directly from the 186 keV photopeak using gamma spectrometry and a neural network, Radiat. Phys. Chem. 217 (2024), https://doi.org/10.1016/j.radphyschem.2023.111486.
[63] J.A. Suárez-Navarro, C. Gascó, M.M. Alonso, M.T. Blanco-Varela, M. Lanzon, F. Puertas, Use of Genie 2000 and Excel VBA to correct for γ-ray interference in the determination of NORM building material activity concentrations, Appl. Radiat. Isot. 142 (2018) 1–7, https://doi.org/10.1016/j.apradiso.2018.09.019.
[64] UNE IE, UNE-EN ISOIEC 170252017. General requirements for the competence of testing and calibration laboratories, (2017).
[65] C. Nuccetelli, S. Risica, M. D'Alessandro, R. Trevisi, Corrigendum: natural radioactivity in building material in the European Union: robustness of the activity concentration index I and comparison with a room model, –259, J. Radiol. Prot. 33 (2013) 259, https://doi.org/10.1088/0952-4746/33/1/259.
[66] BOE, Disposición 21682 del BOE núm. 305 de 2022, 2022. ⟨https://www.boe.es⟩.
[67] I. Gutiérrez-Álvarez, J.E. Martín, J.A. Adame, C. Grossi, A. Vargas, J.P. Bolívar, Applicability of the closed-circuit accumulation chamber technique to measure radon surface exhalation rate under laboratory conditions, Radiat. Meas. 133 (2020) 106284, https://doi.org/10.1016/j.radmeas.2020.106284.
[68] I.S.O., Measurement of radioactivity in the environment-Air: Radon-222-Test methods for exhalation rate of building materials, 2016.
[69] I. López Coto, J.L. Mas, J.P. Bolivar, R. García-Tenorio, A short-time method to measure the radon potential of porous materials, Appl. Radiat. 67 (2009) 133–138, https://doi.org/10.1016/j.apradiso.2008.07.015.
[70] SARAD, RTM 1688-2 Radon-and Thoron-Measurement equipment Referenced documents: Software manual Radon Vision Software manual ROOMS 1.2.0 Content, 2022. ⟨www.sarad.de⟩.
[71] Durrige, Electronic Radon Detector User Manual, 2022.
[72] O. Burgos-Montes, M.M. Alonso, F. Puertas, Viscosity and water demand of limestone- and fly ash-blended cement pastes in the presence of superplasticisers, Constr. Build. Mater. 48 (2013) 417–423, https://doi.org/10.1016/j.conbuildmat.2013.07.008.
[73] Q. Zeng, K. Li, T. Fen-chong, P. Dangla, Determination of cement hydration and pozzolanic reaction extents for fly-ash cement pastes, Constr. Build. Mater. 27 (2012) 560–569, https://doi.org/10.1016/j.conbuildmat.2011.07.007.
[74] M.M. Alonso, M. Palacios, F. Puertas, Compatibility between polycarboxylate-based admixtures and blended-cement pastes, Cem. Concr. Compos 35 (2013) 151–162, https://doi.org/10.1016/j.cemconcomp.2012.08.020.
[75] M.M. Alonso, J.A. Suárez-Navarro, R. Pérez-Sanz, C. Gascó, A.M. Moreno de los Reyes, M. Lanzón, M.T. Blanco-Varela, F. Puertas, Data on natural radionuclide's activity concentration of cement-based materials, Data Brief. 33 (2020), https://doi.org/10.1016/j.dib.2020.106488.
[76] M.Á. Sanjuán, J.A. Suarez-Navarro, C. Argiz, P. Mora, Assessment of radiation hazards of white and grey Portland cements, J. Radio. Nucl. Chem. 322 (2019) 1169–1177, https://doi.org/10.1007/s10967-019-06824-y.
[77] A. Baeza, M. Del Rio, C. Miro, J. Paniagua, Natural Radionuclide Distribution in Soils of Cficeres (Spain): Dosimetry Implications, 1994.
[78] UNSCEAR, Sources and effects of ionizing radiation: United Nations Scientific Committee on the Effects of Atomic Radiation: UNSCEAR 2000 report to the General Assembly, with scientific annexes., United Nations, 2000.
[79] D.J. Karangelos, N.P. Petropoulos, M.J. Anagnostakis, E.P. Hinis, S.E. Simopoulos, Radiological characteristics and investigation of the radioactive equilibrium in the ashes produced in lignite-fired power plants, J. Environ. Radio. 77 (2004) 233–246, https://doi.org/10.1016/j.jenvrad.2004.03.009.
[80] M.Á. Sanjuán, J.A. Suarez-Navarro, C. Argiz, E. Estévez, Radiation dose calculation of fine and coarse coal fly ash used for building purposes, J. Radio. Nucl. Chem. 327 (2021) 1045–1054, https://doi.org/10.1007/s10967-020-07578-8.
[81] M.M. Alonso, J.A. Suárez-Navarro, R. Pérez-Sanz, C. Gascó, A.M. Moreno de los Reyes, M. Lanzón, M.T. Blanco-Varela, F. Puertas, Data on natural radionuclide's activity concentration of cement-based materials, Data Brief. 33 (2020) 106488, https://doi.org/10.1016/j.dib.2020.106488.
[82] J. Miller, J. Miller, Statistics and chemometrics for analytical chemistry, Pearson education, 2018.
[83] M.Á. Sanjuán, B. Quintana, C. Argiz, Coal bottom ash natural radioactivity in building materials, J. Radio. Nucl. Chem. 319 (2019) 91–99, https://doi.org/10.1007/s10967-018-6251-0.
[84] E. Fidanchevski, B. Angjusheva, V. Jovanov, P. Murtanovski, L. Vladiceska, N. S. Aluloska, J.K. Nikolic, A. Ipavec, K. Šter, M. Mrak, S. Dolenec, Technical and radiological characterisation of fly ash and bottom ash from thermal power plant, J. Radio. Nucl. Chem. 330 (2021) 685–694, https://doi.org/10.1007/s10967-021-07980-w.
[85] N. Lauer, A. Vengosh, S. Dai, Naturally occurring radioactive materials in uranium-rich coals and associated coal combustion residues from China, Environ. Sci. Technol. 51 (2017) 13487–13493, https://doi.org/10.1021/acs.est.7b03473.
[86] D.G. Coles, R.C. Ragaini, J.M. Ondov, Behavior of natural radionuclides in western coal-fired power plants, Environ. Sci. Technol. 12 (1978) 442–446, https://doi.org/10.1021/es60140a007.
[87] D.C. Narloch, S.A. Paschuk, J.N. Corrêa, Z. Rocha, W. Mazer, C.A.M.P. Torres, F. Del Claro, V. Denyak, H.R. Schelin, Characterization of radionuclides present in portland cement, gypsum and phosphogypsum mortars, Radiat. Phys. Chem. 155 (2019) 315–318, https://doi.org/10.1016/j.radphyschem.2018.07.011.
[88] W. Kingkam, N. Changkit, R. Samran, S. Nuchdang, D. Rattanapha, Optimization of monazite content in mortar cement and assessment of radiological risk in building materials, Case Stud. Chem. Environ. Eng. 8 (2023), https://doi.org/10.1016/j.cscee.2023.100514.
[89] A. Sakoda, Y. Ishimori, K. Yamaoka, A comprehensive review of radon emanation measurements for mineral, rock, soil, mill tailing and fly ash, Appl. Radiat. Isot. 69 (2011) 1422–1435, https://doi.org/10.1016/j.apradiso.2011.06.009.
[90] S. Stoulos, M. Manolopoulou, C. Papastefanou, Measurement of radon emanation factor from granular samples: effects of additives in cement, Appl. Radiat. Isot. 60 (2004) 49–54, https://doi.org/10.1016/j.apradiso.2003.10.004.

[91] D. Hatungimana, C. Taşköprü, M. İçhedef, M.M. Saç, Yazıcı, Compressive strength, water absorption, water sorptivity and surface radon exhalation rate of silica fume and fly ash based mortar, J. Build. Eng. 23 (2019) 369–376, https://doi.org/10.1016/j.jobe.2019.01.011.
[92] M.Y. Shoeib, D.A. Ahmed, A.F. Abd-Elraheem, A study of 226Ra concentration and radon exhalation rates in different geopolymer cement samples using CR-39 solid state nuclear track detector, Radiat. Phys. Chem. 216 (2024), https://doi.org/10.1016/j.radphyschem.2023.111381.
[93] T. Tene, C. Vacacela Gomez, G. Tubon Usca, B. Suquillo, S. Bellucci, Measurement of radon exhalation rate from building materials: the case of Highland Region of Ecuador, Constr. Build. Mater. 293 (2021), https://doi.org/10.1016/j.conbuildmat.2021.123282.
[94] C. Dueñas, M.C. Fernández, J. Carretero, E. Liger, M. Pérez, Release of 222 Rn from some soils, EGS-Springer-Verlag, 1997.
[95] UNSCEAR, SOURCES, EFFECTS AND RISKS OF IONIZING RADIATION United Nations Scientific Committee on the Effects of Atomic Radiation 1988 Report to the General Assembly, with annexes UNITED NATIONS, 1988.
[96] R.P. Chauhan, A. Kumar, A Comparative Study of Indoor Radon Contributed by Diffusive and Advective Transport through Intact Concrete. Phys Procedia, Elsevier B.V., 2015, pp. 109–112, https://doi.org/10.1016/j.phpro.2015.11.066.
[97] R.P. Chauhan, A. Kumar, Study of radon transport through concrete modified with silica fume, Radiat. Meas. 59 (2013) 59–65, https://doi.org/10.1016/j.radmeas.2013.10.009.
[98] R.P. Chauhan, A. Kumar, Radon resistant potential of concrete manufactured using Ordinary Portland Cement blended with rice husk ash, Atmos. Environ. 81 (2013) 413–420, https://doi.org/10.1016/j.atmosenv.2013.09.024.
[99] A. Kumar, R.P. Chauhan, Active and passive measurements of radon diffusion coefficient from building construction materials, Environ. Earth Sci. 72 (2014) 251–257, https://doi.org/10.1007/s12665-013-2951-5.